plants

MDPI

Review

Photorespiration: The Futile Cycle?

Xiaoxiao Shi and Arnold Bloom *

Department of Plant Sciences, University of California Davis, Davis, CA 95616, USA; xxsshi@ucdavis.edu
* Correspondence: ajbloom@ucdavis.edu; Tel.: +1-530-752-1743

Abstract: Photorespiration, or C_2 photosynthesis, is generally considered a futile cycle that potentially decreases photosynthetic carbon fixation by more than 25%. Nonetheless, many essential processes, such as nitrogen assimilation, C_1 metabolism, and sulfur assimilation, depend on photorespiration. Most studies of photosynthetic and photorespiratory reactions are conducted with magnesium as the sole metal cofactor despite many of the enzymes involved in these reactions readily associating with manganese. Indeed, when manganese is present, the energy efficiency of these reactions may improve. This review summarizes some commonly used methods to quantify photorespiration, outlines the influence of metal cofactors on photorespiratory enzymes, and discusses why photorespiration may not be as wasteful as previously believed.

Keywords: photorespiration; oxygenation; photosynthesis; metal cofactor; atmospheric CO_2; climate change; crop yield; metabolic interactions; kinetics

Citation: Shi, X.; Bloom, A. Photorespiration: The Futile Cycle? *Plants* **2021**, *10*, 908. https://doi.org/10.3390/plants10050908

Academic Editor: Marco Betti

Received: 15 April 2021
Accepted: 29 April 2021
Published: 1 May 2021

1. Introduction

Photorespiration involves the oxygenation of ribulose-1,5-bisphosphate (RuBP) to form 3-phosphoglycerate (3PGA) and 2-phosphoglycolate (2PG) and the subsequent carbon oxidation pathways that release CO_2 under light conditions [1–5]. Because it produces 2PG, a compound "toxic" to many enzymes in photosynthetic metabolism, and oxidizes organic carbon without seemingly generating ATP, photorespiration is generally considered a wasteful process. The following sections examines how the photorespiratory pathway converts 2PG into glycolate, the only carbon source for the photosynthetic carbon oxidation cycle [6], a cycle that together with nitrogen assimilation, C_1 metabolism, and sulfur assimilation generates essential amino acids and intermediate compounds [7]. Moreover, the three enzymes involved in the initial photorespiratory steps within chloroplasts—Rubisco, malic enzyme, and phosphoglycolate phosphatase—have metal binding sites that accommodate either Mg^{2+} or Mn^{2+}, and balance between the binding of these enzymes to Mg^{2+} or Mn^{2+} may shift the relative rates and energy efficiencies of photosynthesis and photorespiration [8].

2. Photosynthesis vs. Photorespiration

2.1. Rubisco

Atmospheric CO_2 concentration has increased more than 20% during the past 35 years [9]. The major sink for this CO_2 is the approximately 258 billion tons per year that photosynthetic organisms convert into organic carbon compounds through carbon fixation via the Calvin–Benson pathway [10]. This pathway begins with Rubisco (Ribulose 1,5-bisphosphate carboxylase–oxygenase), the most abundant protein on the planet [11].

Rubisco comes in three forms [12]:

Form I, which is found in cyanobacteria, proteobacteria, chlorophyte algae, heterokont algae, and haptophyte algae, and higher plants, is the most common [13,14]. It is a hexadecamer containing eight identical large subunits (~55,000 M_r), each with a metal-binding site, and eight small subunits (~15,000 M_r). The large subunits are coded by a single

plastomic gene, whereas the small subunits are coded by a nuclear multigene family that consists of 2 to 22 members, depending on the species [15]. Complex cellular machinery is required to assemble this form of Rubisco and to maintain its activity [16]. Form I Rubisco, until recently, had resisted all efforts to generate a functional holoenzyme in vitro or upon recombinant expression in *E. coli* [17].

Form II Rubisco, found in proteobacteria, archaea, and dinoflagellate algae, contains one or more isodimers with subunits that share about 30% identity to the large subunit of Form I Rubisco [8].

Form III Rubisco, found in archaea, has one or five isodimers composed of subunits homologous to the large subunit of Form I Rubisco [8].

Form II and Form III Rubisco show greater similarity in their primary sequence to one another than either do to the large subunit of Form I Rubisco [8].

All three forms of Rubisco catalyze not only the reaction in which the carboxylation of the five-carbon sugar RuBP generates two molecules of the three-carbon organic acid 3-phosphoglycerate (3PGA), but also an alternative reaction in which oxidation of RuBP generates one molecule of 3PGA and one of 2PG (Figure 1) [8]. The carboxylation pathway of photosynthesis expends 3 ATP and 2 NADPH per RuBP regenerated and produces a carbon in hexose [18], whereas the oxygenation pathway of photorespiration reportedly expends 3.5 ATP and 2 NADPH per RuBP regenerated but produces no additional organic carbon [19,20].

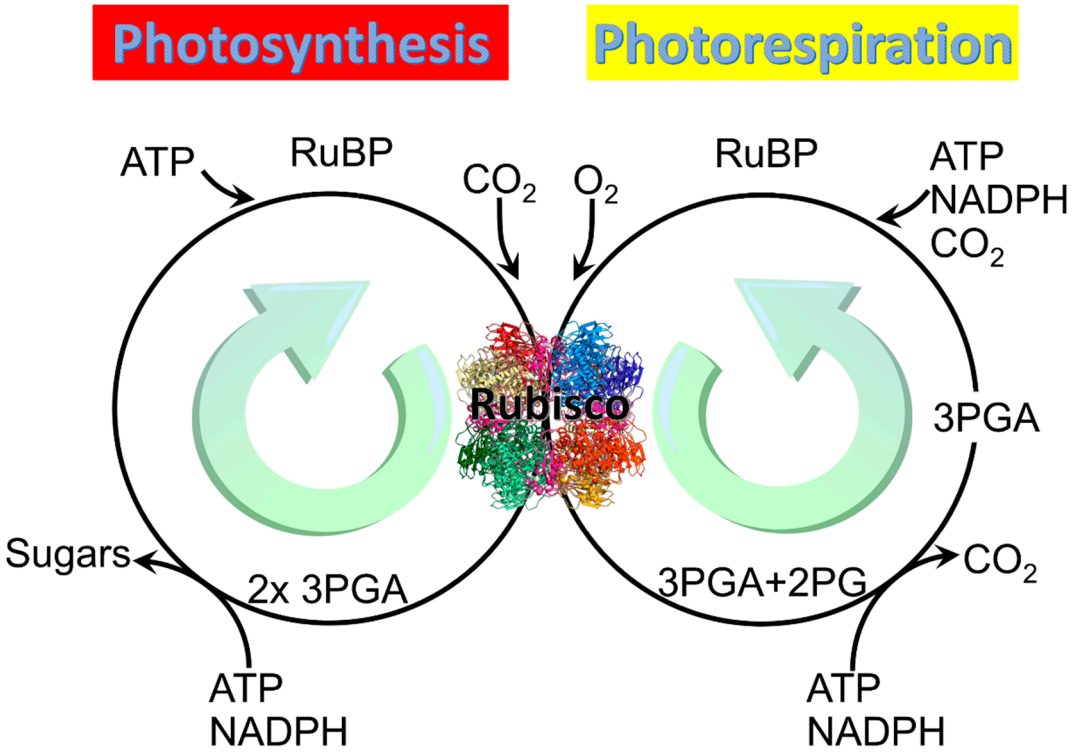

Figure 1. Two main reactions of Rubisco: Photosynthesis and photorespiration. Rubisco structure picture credit: Laguna design / science photo library.

Rubisco must be activated before it can carboxylate or oxygenate RuBP. Activation of the three forms of Rubisco involves binding of Mn^{2+} or Mg^{2+} [21,22]. Binding of Mg^{2+} requires carbamylation of Rubisco by the addition of CO_2. One histidine at the active site of Rubisco rotates into an alternate conformation, resulting in a transient binding site where Mg^{2+} is partially neutralized by the conversion of two water molecules to hydroxide ions and coordinated indirectly by three histidine residues through the water molecules. Subsequently, the hydroxide ions cause a lysine residue at the active site to

become deprotonated and rotate 120 degrees into the *trans* conformer, which brings its nitrogen into close proximity to the carbon of CO_2, allowing for the formation of a covalent bond that produces a carbamyl group. This carbamyl group causes the Mg^{2+} ion to transfer to a second binding site, after which the histidine that first rotated returns to its original conformation [23]. It is unclear whether binding Mn^{2+} follows a similar mechanism and whether it requires an activator CO_2 to be bound first [21,22]; hence, understanding the mechanism of Mn^{2+} binding to Rubisco is important to future research on Rubisco kinetics. During in vitro studies, Rubisco is often activated at pH 8.0 in the presence of CO_2 and either Mg^{2+} or Mn^{2+}.

Rubisco can also bind to other metals. When bound to Fe^{2+}, Ni^{2+}, Cu^{2+}, Ca^{2+}, or Co^{2+}, Rubisco may exhibit some carboxylase and oxygenase activity [24]. For example, one study found that Rubisco from *R. rubrum*, when bound to Co^{2+}, was incapable of carboxylation but still capable of oxygenation [24]. Another study found that Rubisco from spinach performed both carboxylation and oxygenation when bound to Ni^{2+} or Co^{2+} [25]. When bound to some other metal ions, including Cd^{2+}, Cr^{2+}, and Ga^{2+}, Rubisco cannot catalyze either carboxylation or oxygenation [24]. Although it is known that the metal ion plays a role in stabilizing the activator carbamate and determining the active site's structure, its effect upon the reactions catalyzed by Rubisco is still not completely understood. One hypothesis is that Mg^{2+}, because of its electron-withdrawing properties, polarizes the C2 carbonyl of RuBP, which favors the removal of the C3 proton and thereby contributes to enolization [21].

NADPH complexes strongly with Rubisco and acts as an effector molecule to maintain the Rubisco catalytic pocket in an open confirmation that more rapidly facilitates CO_2-Mg^{2+} activation when CO_2 and Mg^{2+} are present in suboptimal concentrations [26–29]. The crystal structure of Rubisco with both Mg^{2+} and NADPH as ligands indicates that NADPH binds to the catalytic site of Rubisco through metal-coordinated water molecules [26]. The activated enzyme catalyzes either carboxylation or oxygenation of the enediol form of the five-carbon sugar ribulose-1,5-bisphosphate (RuBP) [14,21,22,30,31].

2.2. Balance between Carboxylation and Oxygenation and Metal Cofactors

Several factors alter the balance between Rubisco carboxylation and oxygenation and, thereby, alter the relative rates of photosynthesis and photorespiration. These include the concentrations of CO_2 and O_2 at the active site of Rubisco, the specificity of the enzyme for each gas, and whether the enzyme is associated with Mg^{2+} or Mn^{2+} [32]. These divalent cations share the same binding site in Rubisco [14,22,33], and in tobacco, Rubisco associates with both metals and rapidly exchanges one metal for the other [32]. Nonetheless, nearly all recent studies on the photosynthetic and photorespiratory pathways have been conducted in the presence of Mg^{2+} and absence of Mn^{2+} [8]. Rubisco binding of Mg^{2+} accelerates carboxylation, whereas binding of Mn^{2+} slows carboxylation [25,34–38]. Chloroplastic Mg^{2+} and Mn^{2+} activities seem to be regulated at the cellular level because in isolated tobacco chloroplasts, activities of the metals were directly proportional to their concentrations in the medium [32]. The thermodynamics of binding Mg^{2+} to Rubisco were similar for enzymes isolated from a Form I and a Form II species [32]. By contrast, the thermodynamics of binding differed greatly between the two Rubisco forms when the enzymes were associated with Mn^{2+} [32].

Mg^{2+} and Mn^{2+} have nearly identical ionic radii but highly disparate electron configurations: Mg^{2+} ($1s^2 2s^2 2p^6$ or [Ne]) has a very stable outer shell [8], whereas Mn^{2+} has five unpaired d electrons ($1s^2 2s^2 2p^6 3s^2 3p^6 3d^5$ or [Ar]$3d^5$) that are susceptible to many redox reactions. An aerated solution of activated Mn^{2+}-Rubisco exhibits a long-lived chemiluminescence when RuBP is added [39,40]. This chemiluminescence was attributed to a spin-flip within the Mn^{2+} 3d manifold, leading to an excited quartet ($S = {}^3/_2$) d^5 electronic configuration that decays over the course of 1 to 5 min back to the sextet ($S = {}^5/_2$) ground state electronic configuration [39]. Excited states are intrinsically better oxidants and reductants (larger reduction/oxidation potentials) than their corresponding ground

states [41–43]; thus, the observed chemiluminescence opens the possibility that the RuBP-O_2-Mn^{2+}—Rubisco excited state may be quenched via electron transfer. Consequently, the liberated reducing equivalent could participate in the reduction of $NADP^+$ to NADPH (Figure 2, blue pathway). In this way, oxidation of RuBP via O_2 may proceed in a spin-allowed manner, while the Mn^{2+} remains "innocent" in the generation of the oxygenated RuBP precursor. Mn^{2+}-centered redox may still proceed, with oxidation of excited Mn^{2+} to Mn^{3+} occurring in a manner independent of, but parallel to, substrate oxidation.

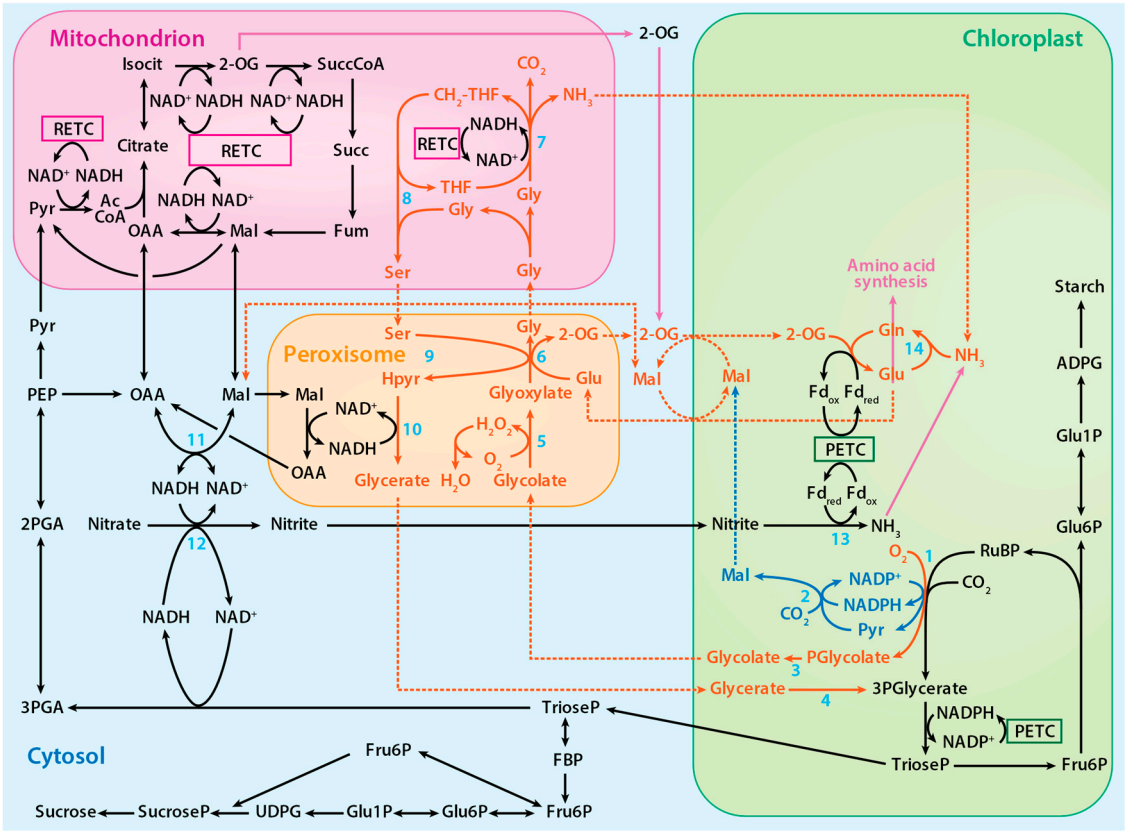

Figure 2. The proposed photorespiratory pathway within the context of photosynthetic carbon and nitrogen metabolism. The solid red lines represent reactions of the photorespiratory pathway, the solid blue lines represent reactions of the proposed alternative photorespiratory pathway, the solid purple lines represent reactions of amino acid synthesis, and the dotted lines represent associated transport processes. Numbered reactions are catalyzed by the following enzymes: 1. Rubisco, 2. Malic enzyme, 3. Phosphoglycolate phosphatase, 4. Glycerate kinase, 5. Glycolate oxidase, 6. Glutamate:glyoxylate aminotransferase, 7. Glycine decarboxylase complex, 8. Serine hydroxymethyltransferase-1, 9. Serine:glyoxylate aminotransferase, 10. Hydroxypyruvate reductase-1, 11. Malate dehydrogenase, 12, Nitrate reductase, 13 Nitrite reductase, and 14. Glutamine synthetase. PETC designates photosynthetic electron transport chain and RETC, respiratory electron transport chain. Adapted from ref. [8]. Copyright 2018 Springer Nature Ltd.

In wheat leaves, the ratio of Mn^{2+} to Mg^{2+} contents increased as the CO_2 levels increased and when the nitrogen source was nitrate rather than ammonium [32]. Nitrate assimilation into amino acids in shoots is heavily dependent on photorespiration, whereas ammonium assimilation is much less so. This indicates that plants shifted to Rubisco Mn^{2+} binding in order to compensate for the slower photorespiration rates and slower amino acid production that would otherwise occur under elevated CO_2 and nitrate nutrition.

2.3. The Photorespiratory Pathway

The 3-phosphoglycerate produced during photorespiration, like that produced during photosynthesis, is converted to triose phosphate and used to regenerate RuBP. On the other hand, 2-phosphoglycolate is converted to glycolate by phosphoglycolate phosphatase. In

the peroxisome and mitochondrion, a series of reactions converts glycolate to glycerate, which is ultimately returned to the chloroplast to regenerate RuBP (Figure 2) [8]. In addition to Rubisco, several other chloroplast enzymes in the photorespiratory pathway, including malic enzyme and phosphoglycolate phosphatase, bind either Mg^{2+} or Mn^{2+} [8]. The plastid isoform of malic enzyme in *Arabidopsis* and tobacco catalyzes the reverse pyruvate synthesis reaction (pyruvate + CO_2 + NADPH → malate + NADP) [44,45]. Phosphoglycolate phosphatase, which is responsible for the hydrolysis of 2-phosphoglycolate to glycolate, binds to and is activated by either metal [46]. Hypothesized is an alternative photorespiratory pathway that increases photorespiration energy efficiency by generating malate (RuBP + O_2 + CO_2 + H_2O → glycolate + malate + 2Pi) when Mn^{2+} binds to these enzymes (Figure 2) [8].

3. Estimating Rates of Photorespiration

Many different methods have been employed for estimating rates of photorespiration. The following sections outline the general approach of each method and highlights the assumptions and potential errors in each. The hope is that certain methods might be better suited for assessing the influence of Mn^{2+} vs. Mg^{2+} on the relative rates of oxygenation and carboxylation in situ.

3.1. Traditional Methods for Estimating Photorespiration

3.1.1. Post Illumination CO_2 Burst

This method measures the evolution of CO_2 from a leaf for 1 to 4 min after turning off the light because glycine metabolism continues longer in the dark than CO_2 assimilation [47]. The rate of CO_2 generation is measured by a transient CO_2 analyzer [48] when the light has just been turned off or at the maximum rate of CO_2 evolution observed. CO_2 assimilation, however, does not stop immediately after the light is off. Separating CO_2 assimilation from the CO_2 burst effects during this time is difficult, and hence this method underestimates photorespiratory rates [49,50]. This method also fails to consider variations in mitochondrial respiration, leading to overestimates of photorespiratory rates [51].

3.1.2. O_2 Inhibition of Net CO_2 Assimilation

This method aims to assess the photorespiration rate from the increase in the CO_2 assimilation rate after switching from normal to low O_2 concentrations. Yet, changes in CO_2 assimilation with O_2 concentration may derive from components of the photosynthetic pathway other than photorespiration [4]. For example, when starch and sucrose synthesis limit photosynthesis, increasing or decreasing the photorespiration does not affect net CO_2 assimilation [52].

3.1.3. Photorespiration CO_2 Efflux into CO_2-Free Air

This method estimates photorespiration from the CO_2 efflux rate in CO_2-free air. A high-O_2 and low-CO_2 environment, however, promotes photorespiration [4]. Additionally, a CO_2-free atmosphere inhibits both the activity of Rubisco [53] and the regeneration of its substrate RuBP [54], leading to underestimates of photorespiration.

3.1.4. Ratio of $^{14}CO_2$ to $^{12}CO_2$ Uptake

In this method, $^{14}CO_2$ and $^{12}CO_2$ fluxes are measured after feeding a leaf with $^{14}CO_2$ for a short period of time. Gross photosynthesis is estimated from $^{14}CO_2$ uptake measured using an ionization chamber attached to an electrometer, while net photosynthesis is estimated from $^{12}CO_2$ measured using an infrared gas analyzer. Photorespiration is estimated as the difference between gross and net photosynthesis [55] (Figure 3).

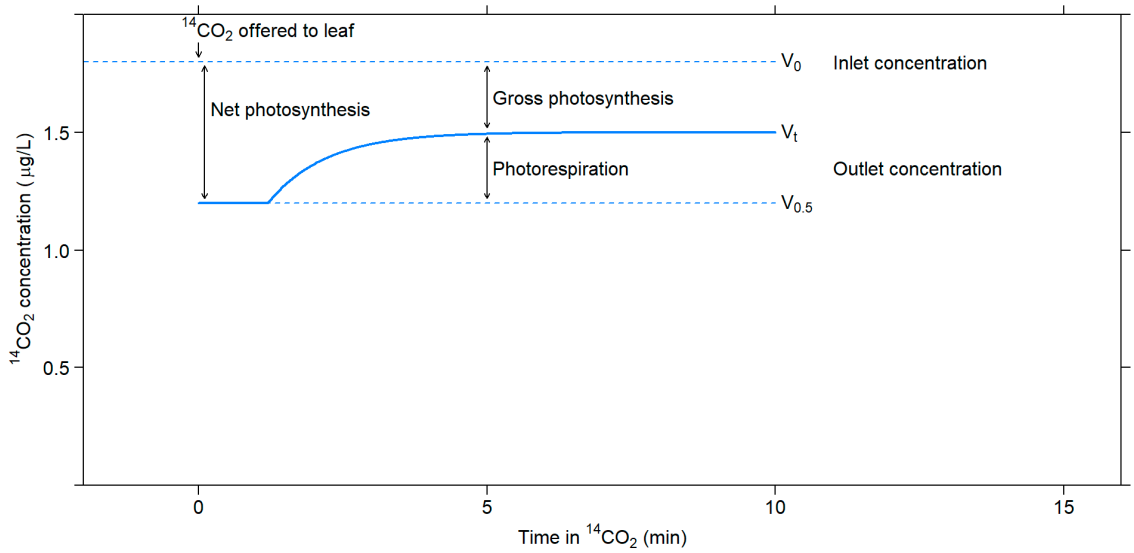

Figure 3. Changes in $^{14}CO_2$ concentration that occur upon exposing a leaf in the light to $^{14}CO_2$. Adapted with permission from ref. [55]. Copyright 1971 Canadian Science Publishing.

There are several uncertainties associated with this method. The recycling effect on the specific activity of CO_2 inside the leaf can cause about a 20% error. One must consider the specific activity of CO_2 inside the leaf to obtain an accurate estimate of the gross photosynthesis rate because CO_2 efflux through photorespiration dilutes the ^{14}C label in the intercellular spaces, decreasing the specific activity of CO_2. The activity might be even lower at the actual carboxylation site than in the interleaf spaces because of photorespiratory CO_2 loss [56]. Moreover, Rubisco carboxylation discriminates about 2.9% against ^{13}C [57,58] and about 5.5% against ^{14}C [4], resulting in errors in estimations of photorespiration rates that exceed 25% [4,57].

3.2. Recent Methods for Estimating Photorespiration

3.2.1. Calculation from Kinetics Models

Rubisco reaction kinetics can provide an estimate of the photorespiration rate [4,59]. This method can provide accurate estimates of photorespiration rates if the CO_2 compensation point in the absence of mitochondrial respiration (**Γ***) being known for a given plant species. The rate of oxygenation, which is assumed to be twice the rate of photorespiration, is given by:

$$v_o = \frac{A + R_d}{\frac{1}{\Phi} - 0.5}$$

where A is the rate of photosynthetic CO_2 assimilation, R_d is the rate of respiration other than photorespiration, and:

$$\Phi = \frac{v_o}{v_c} = \frac{2\Gamma^*}{C}$$

where C is the CO_2 concentration.

The principal drawbacks of this method are that it does not directly measure photorespiration and depends on estimates of C and Γ*. There are several techniques for estimating C at the site of Rubisco activity, but estimating Γ* is more difficult. Values for Γ* are known for only a few species, and depend on estimates of kinetic parameters, which themselves rely on estimates of photorespiration [59].

3.2.2. CO_2 Efflux into $^{13}CO_2$-Air

The gas exchange method is based on the FvCB (Farquhar, van Caemmerer, and Berry) model [4,59]. First, ambient air is rapidly replaced with air containing $^{13}CO_2$ and no $^{12}CO_2$.

The levels of released $^{12}CO_2$ can be measured either using an infrared gas analyzer or a membrane inlet mass spectrometer. Because the rate of $^{12}CO_2$ release includes both photorespiration and mitochondrial respiration, additional effort is needed to separate these effects. For example, in one approach, the rate of $^{12}CO_2$ release is calculated as:

$$R_{12_C} = \frac{F\left({}^{12}C_R - {}^{12}C_S \frac{1-W_R}{1-W_S}\right)}{a}$$

where F is the gas flow rate, ${}^{12}C_R$ and ${}^{12}C_S$ are the mole fractions of $^{12}CO_2$ in the chamber without and with a leaf, W_R and W_S are the corresponding water mole fractions, and a is the illuminated leaf area in the chamber [60]. To divide this quantity into photorespiration and mitochondrial respiration, the air is replaced with air containing 10,000 ppm $^{13}CO_2$ and the concentration of $^{13}CO_2$ over 2 min is fitted to an exponential curve. The mitochondrial respiration R_d is taken to be the rate of $^{12}CO_2$ release after 2 min.

This method can provide estimates of both carboxylation and oxygenation if one assumes that the rate of mitochondrial respiration (R_d) is not affected by the sudden high CO_2 concentration, that 0.5 CO_2 is generated per oxygenation reaction when the CO_2 released per oxygenation varies widely with temperature and light level and among species [7], and that leaves do not naturally contain any ^{13}C [59]. If intracellular reassimilation is significant and it often is [60], substantial errors in the estimate can result. These errors can be accounted for by monitoring the release of $^{12}CO_2$ after switching from ambient air to air with a high concentration of $^{13}CO_2$; however, high CO_2 concentrations could affect mitochondrial respiration and thus produce error in the estimate of photorespiration. The presence of naturally occurring ^{13}C also generates additional errors [59].

3.2.3. Labelling of Photosynthates with ^{14}C

Leaves at a photosynthetic steady state are exposed to $^{14}CO_2$ for different lengths to label primary and stored photosynthates. Exposing the leaf to an ambient concentration of $^{14}CO_2$ for 10 to 15 min will label primary photosynthates, such as the metabolites from the Calvin cycle, glycolate cycle, and intermediates of starch and sucrose synthesis and of glycolysis [44]. Longer exposures (2 to 3 h) will label stored photosynthates, such as starch, sucrose, fructans, and vacuolar acids. $^{14}CO_2$ efflux into different backgrounds containing various combinations of O_2 and CO_2 concentrations provides an estimate of photorespiration [61,62]. Four different backgrounds are used: first, 21% O_2 and ambient CO_2 to measure the steady-state release of CO_2 from both photosynthesis and photorespiration; second, 1.5% O_2 and ambient CO_2 to measure the rate of photorespiration only; third, 21% O_2 and 30,000 µmol/mol CO_2 to limit CO_2 reassimilation; and fourth, 21% O_2 with no CO_2 to measure the specific radioactivity of CO_2 efflux [63].

The assumptions for this method are that all photosynthates must be labeled during the labeling time frames and that R_d is not affected by the percentage of O_2 in the air. A recent report indicated that R_d was actually lower at a lower O_2 concentration (2%) than at an ambient concentration (21%) [64]. One also has to assume that the mitochondrial respiration (R_d) value does not change upon transient exposure to high CO_2 levels.

3.2.4. Measuring Photorespiratory Ammonia

Photorespiration generates NH_3 in addition to CO_2 during the conversion from glycine to serine in mitochondria [65]. Adding glutamine synthetase (GS) inhibitors methionine sulphoximine [35] or phosphinothricin [66] prevents ammonia reassimilation in chloroplasts, and NH_3 subsequently accumulates in the leaf. The advantages of this method also include the prevention of CO_2 refixation and uncertainties in R_d values under the experimental conditions [35,66]. This approach, however, depends on several assumptions: (1) The GS inhibitors do not inhibit photorespiration, and (2) they can prevent NH_3 refixation completely.

Other factors might limit the diffusion of NH_3 out of the leaves, leading to an underestimation of photorespiration [59]. GS inhibitors will disrupt the C_2 cycle under photorespiratory conditions, and glycolate will rapidly accumulate, which in turn will inhibit photosynthesis. Feeding the plant an amino acid donor, such as glutamine, together with GS inhibitors will help minimize this inhibition effect [66,67].

Quantification of ammonia poses some challenges. The commonly used ion chromatography method to quantify NH_4^+ may overestimate the amount of NH_4^+ because methylamine, ethylamine, ethanolamine, and some non-protein amino acids co-elute with NH_4^+. Degradation of labile nitrogen metabolites in leaf extract, xylem sap, and apoplastic fluid to NH_4^+ during extraction will cause further overestimation of NH_4^+ levels [68].

3.2.5. Measuring $^{18}O_2$ Consumption and Labeled Metabolites

Replacing ambient air in a chamber containing a leaf with air containing $^{18}O_2$ provides another estimate of the photorespiration rate. A mass spectrometer measures levels of $^{16}O_2$ and $^{18}O_2$. The rate of oxygenation is estimated as:

$$v_o = \frac{2}{3}\left(^{18}O_2 \; uptake \; in \; light - \; ^{18}O_2 \; uptake \; in \; dark\right)$$

and carboxylation as:

$$v_c = \; ^{16}O_2 \; evolution - v_o$$

Ref. [69,70].

Unfortunately, this method cannot separate photorespiration from other light-dependent O_2-consuming processes, such as light-dependent differences in the rate of mitochondrial respiration [46,48]. To diminish these errors, the mass spectrometer can quantify ^{18}O-labeled metabolites, such as glycolate, glycine, and serine; with several assumptions about the photorespiratory pathway, such as the pool sizes of the labeled metabolites [49], one can then use the amounts of labeled metabolites to calculate the photorespiration rate [71,72].

3.2.6. NMR Measurements on ^{13}C-Labeled Metabolites

This method requires that plants receive fertilizer labeled with ^{15}N and that leaves subsequently be exposed to $^{13}CO_2$. Rotational-echo double resonance (REDOR) detects ^{13}C within two covalent bonds of ^{15}N and thus assesses the formation of organic nitrogen metabolites labeled with ^{13}C [59,73]. The ratio of ^{13}C-labeled to unlabeled phosphorylated Calvin–Benson cycle metabolites between 2 and 4 min after exposure to $^{13}CO_2$ indicates the ratio of photosynthesis to photorespiration [50]. This assumes that metabolites produced from photosynthesis are fully labeled in less than 2 min after being exposed to $^{13}CO_2$ and that those produced from photorespiration do not become labeled until after 4 min. These assumptions may lead to errors because photosynthesis may re-assimilate some of the $^{12}CO_2$ generated by photorespiration and because photorespiration may produce intermediates labeled with ^{13}C in less than 2 min [60]. Furthermore, this method is based on the premise that photorespiration releases one CO_2 for every two oxygenations, when the CO_2 released per oxygenation varies widely with temperature and light level and among species [7].

3.2.7. Quantification of 2-Phosphoglycolate (2PG) and Photorespiratory Metabolites by Mass Spectrometry

This method uses LC-MS/MS to measure directly the first intermediate, 2PG, of photorespiration when Rubisco oxygenates RuBP, and GC-MS to measure other photorespiratory metabolites. In the LC-MS/MS portion, 2PG is separated from other molecules in three steps: First, liquid chromatography separates 2PG based on its physiochemical properties; second, mass spectrometry separates 2PG based on its *m/z* ratio; and third, mass spectrometry separates 2PG based on its *m/z* ratio after being fragmented [74]. Readings from the LC-MS/MS samples are compared with 2PG standard solutions [75]. Addition-

ally, GC-MS is used to quantify additional photorespiratory metabolites, such as glycolate, glyoxylate, glycine, serine, hydroxypyruvate, and glycerate [74,76].

This approach has estimated photorespiratory rates in plant mutants deficient in expression of genes coding for photorespiratory enzymes. The gaseous environment of the aerial part of the plant, but not the root, was altered before experimentally determining the changes in the metabolite (2PG) content [77–81].

This method has several problems [74,82–85]. First, non-volatile salts and metabolites were deposited at the inlet of MS/MS after eluting from the LC step, which is very common when using anion-exchange chromatography [84]. Second, numerous metabolites eluted from the LC step had overlapping and asymmetrical peaks resulting from the matrix effect (interference in the ionization between compounds with similar elution times) [82,85], which significantly affects the sensitivity and accuracy of the measurements on a specific metabolite, such as 2PG. Third, post-harvest changes in metabolite concentrations can severely affect the quantification of 2PG [74,83]. Fourth, the GC-MS step is not targeted and therefore is potentially prone to error if other compounds with a similar molar mass as the photorespiratory metabolites are present [76].

3.2.8. CO_2 Labeling and MS Analysis

Isotopically nonstationary metabolic flux analysis (INST-MFA) can trace ^{13}C-labeled photorespiratory metabolites in plants exposed to $^{13}CO_2$ to assess the photorespiration rate [86–90]. Monitoring the isotope incorporation in downstream metabolites over time assesses the relative contributions of different pathways after administration of the tracer. The turnover rates of each enzyme determine the labeling dynamics (Figure 4). Mathematical metabolic models specific for each pathway are often used to enumerate mass and isotopomer balances and ensure atoms' conservation within the system. The models' proposed metabolic fluxes are compared with those measured experimentally, and differences are minimized with each subsequent iteration.

The INST-MFA approach presents several challenges. A minimum of three sample time points is needed for precise measurements of metabolic fluxes [91]. This makes experimental design more complex and time-consuming. To ensure accurate and precise measurements, the pool size for each component of a metabolic pathway has to be very specific. Absolute quantification of intracellular pool sizes, however, is not yet possible even with pool size measurements made with optimized mathematical modeling [91]. A second challenge of this approach is isotopic transients. Some intracellular metabolites can exhibit short isotopic transients that last only for a few minutes or seconds. Rapid sampling and quenching have to be achieved to obtain precise and meaningful INST-MFA measurements [92].

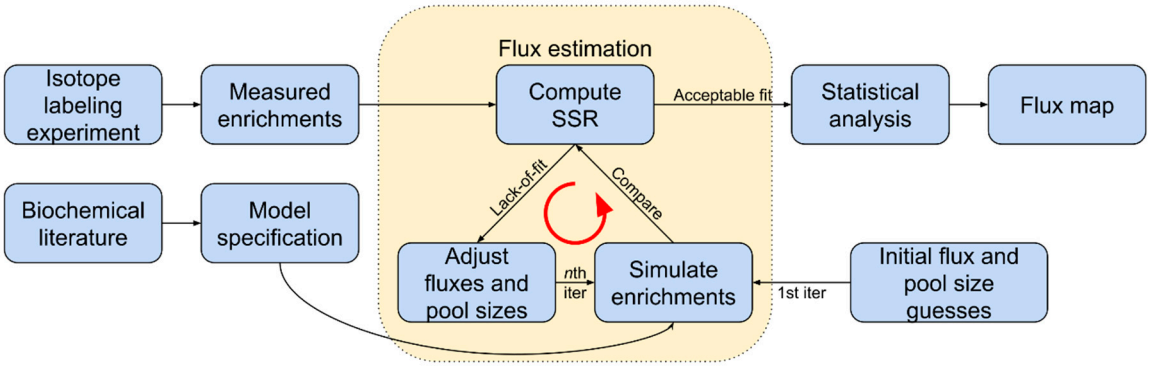

Figure 4. Simplified INST-MFA workflow to estimate flux. Software, such as INCA and OpenMebius, is used in several steps. Fluxes and pool sizes are initially guessed and then adjusted in each iteration, converging upon a flux map that fits measurements of metabolism during the ILE. Adapted with permission from ref. [92]. Copyright 2018 Elsevier Ltd.

3.2.9. Micro-Optode Measurement of O_2 Consumption

We have been conducting direct oxygenation rate measurements using a needle-type O_2 micro-optode to examine the effects of metal cofactors on Rubisco photorespiration reactions. In this instrument, a polymer optical fiber transmits the excitation wavelength to the tip of the sensor and at the same time transmits the fluorescence response of an oxygen-sensitive dye that is immobilized in a polymer matrix at the tip. The rate of oxygenation can be calculated easily by comparing the amount of quenching of the excitation light by dissolved O_2. The micro-optode has a 50–70-µm tip diameter, which makes it possible for a micro-scale setup, such as in a micro-cuvette or plate. The most important advantages for this type of sensor are that the micro-optode does not consume O_2 in contrast to the other commonly used O_2 sensors, such as a Clark electrode [93,94]; it has no stirring sensitivity; and it is resistant to most corrosive environments. The micro-optode also works in both gas (%O_2) and liquid phases (DO), which makes it possible to measure O_2 exchanges accurately up to 250% air O_2 saturation in intact plant leaves, bioreactors, cell cultivation, microtiter plates, and many general oxygen measurements in liquids [95–100].

4. Photorespiration and Other Metabolic Pathways

4.1. NO_3^- Assimilation

Multiple lines of evidence link shoot NO_3^- assimilation to photorespiration:

(a) Elevated CO_2 or low O_2 levels inhibited shoot NO_3^- reduction [101].
(b) In independent ^{14}N and ^{15}N labeling experiments, assimilation of either ^{14}N–NO_3^- or ^{15}N–NO_3^- decreased under CO_2 enrichment [102].
(c) Under elevated CO_2 conditions, NO_3^- nutrient absorption and organic N accumulation levels in various plant species declined when plants received NO_3^- as a sole N source [102–106].
(d) C_3 plants receiving NO_3^- as their sole N source experienced slower growth under CO_2 enrichment than those receiving NH_4^+ [9,107,108].

In wheat and *Arabidopsis* plants grown under CO_2 enrichment and receiving NO_3^- containing ^{15}N at natural abundance levels, shoot tissues became less enriched with ^{15}N organic compounds [102,109]: elevated CO_2 inhibited shoot NO_3^- reduction so it was less limited by nitrate availability, and NO_3^- reductase discriminated more strongly against ^{15}N–NO_3^- [110].

The assimilatory quotient (*AQ*) is the ratio of net CO_2 consumption to net O_2 evolution in plant shoots [111]. During shoot NO_3^- assimilation, ferredoxin generated from the photosynthetic electron chain reduces NO_2^- to NH_4^+ rather than producing NADPH, and so net O_2 evolution increases without a change in net CO_2 consumption. Therefore, the change in assimilatory quotient (ΔAQ) when a plant receives NH_4^+ instead of NO_3^- as a sole N source provides an estimate of shoot NO_3^- assimilation [106]. ΔAQ decreased as the shoot internal CO_2 concentration increased in C_3 plants (Figure 5) [9,104,112,113].

Shoot CO_2 and O_2 fluxes at ambient and elevated CO_2 were contrasted between stages of plant development or genotypes that have significantly different NO_3^- reductase activities in situ (i.e., 36- vs. 48-day-old wild-type *Arabidopsis*, *Arabidopsis* NO_3^- reductase knockout mutants vs. transgenic *Arabidopsis* overexpressing NO_3^- reductase, and NO_3^- reductase-deficient barley mutants vs. wild-type barley) [104,112]. ΔAQ, a measure of shoot NO_3^- assimilation, differed between these stages of development and genotypes under ambient CO_2 but not under elevated CO_2. This indicates that none of the stages of development or genotypes were assimilating NO_3^- under elevated CO_2 [104,112].

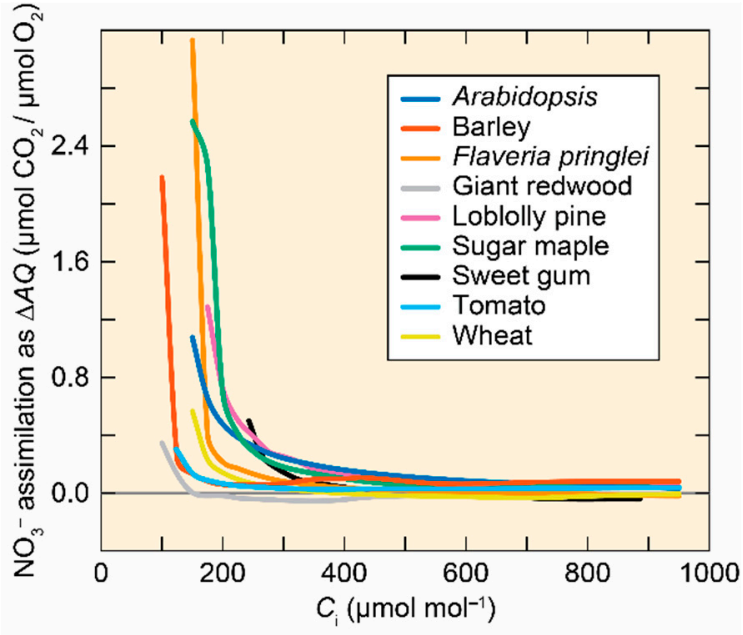

Figure 5. Shoot NO_3^- assimilation as a function of shoot internal CO_2 concentration (C_i) for 9 C_3 species. Adapted with permission from ref. [101]. Copyright 2014 Springer Science Business Media Dordrecht.

Maximum NO_3^- reductase activity in vitro generally declined under CO_2 enrichment [105,114]. Nonetheless, shoot NO_3^- reductase activity seldom limits NO_3^- assimilation in planta [115,116]. Accordingly, NO_3^- assimilation significantly declined only in genotypes with mutations that nearly eliminated enzyme activities [104,117,118], and genotypes with 50% higher NO_3^- reductase activities did not assimilate more NO_3^- [119]. Studies that have confused rates of enzyme activities with those of NO_3^- assimilation as a whole have drawn false conclusions [120,121].

One physiological mechanism that may be responsible for the interdependency of photorespiration and shoot NO_3^- assimilation involves the reduction of the Mn^{2+}-RuBP complex during oxidation of RuBP. This increases the redox potential of the chloroplast [101], thereby stimulating the production of malate [122,123] and promoting its export from chloroplasts to the cytoplasm. Malate dehydrogenase in the cytoplasm converts malate to oxaloacetate, generating NADH [124–126] to empower the initial step of NO_3^- assimilation [127]. Consequently, mutations that alter malate transport or metabolism influence both photorespiration and NO_3^- assimilation [122,128,129].

4.2. C_1 Metabolism

The photorespiratory pathway within mitochondria involve reactions with glycine. In one reaction, serine hydroxymethyltransferase 1 (SHMT1) converts glycine to serine and converts CH_2-THF (5,10-methylene-tetrahydrofolate) to THF (Figure 2). In the other reaction, the glycine decarboxylase complex reduces NAD^+ to NADH and catabolizes glycine to CO_2, NH_3, and CH_2-THF (Figure 2). These C_1 units, in the form of CH_2-THF, serve as precursors in the synthesis of tetrahydrofuran (THF) derivatives [130–133]. One derivative of CH_2-THF, 5-CH_3-THF, is used to produce methionine, an essential amino acid. Methionine is a powerful antioxidant and is involved in protein synthesis and methylation of DNA, RNA, proteins, phospholipids, and other substrates [132]. In addition, about 5% of the total assimilated carbon in many secondary metabolites, such as glycine betaine, nicotine, and lignin, derive from C_1 metabolism [131].

4.3. Sulfur Assimilation

Photorespiration stimulates sulfur assimilation, although the effects are relatively small. By tracing ^{33}S in reactions involved in sulfur assimilation (such as sulfate reduction and synthesis of cysteine), and ^{13}C in glycine and serine, a positive linear relationship was derived between relative photorespiration and sulfur assimilation. Sulfur assimilation decreases as photorespiration declines and photosynthesis increases [134].

Cysteine, the major product from sulfur assimilation, uses the sulfur element converted from serine generated from photorespiratory pathways [134,135]. H_2S, produced from sulfite reduced by sulfite reductase, is incorporated into O-acetylserine (OAS) via a protein complex consisting of serine acetyl transferase and OAS thiol-lyase to form cysteine [135,136]. Cysteine is essential in methionine synthesis, glutathione metabolism, sulfur-rich protein synthesis, glucosinolate biosynthesis, and the synthesis of phytoalexins (Figure 6) [137]. Cysteine is the precursor of methionine through *o*-phosphohomo-serine and homocysteine. Using methyl tetrahydrofolate as a cofactor, homocysteine is methylated by methionine synthase to yield methionine. Cysteine and methionine are the major sulfur contributors found in downstream metabolites, the most important of which is S-adenosyl methionine (SAM), which is a donor in methyl group transfers, transsulfuration, and aminopropylation [135,138].

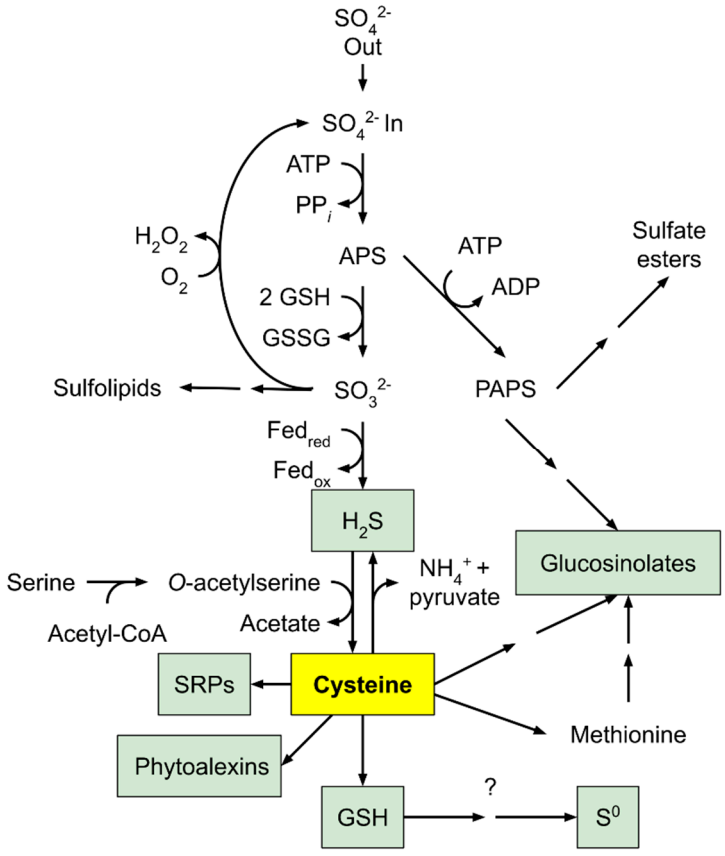

Figure 6. An outline of sulfur assimilation and its role in producing sulfur-containing defense compounds. Adapted with permission from ref. [137]. Copyright 2005 Elsevier Ltd.

5. Conclusions

Is photorespiration simply a futile cycle? The answer is "no". Multiple lines of evidence show its crucial role in many plant processes. Despite heroic efforts to suppress photorespiration, disrupting any photorespiratory reaction usually proves detrimental to plants [139,140]. The reassimilation of CO_2 from photorespiration [60] and the important role played by photorespiration in the acclimation of plants to conditions, such as salin-

ity [141] and elevated CO_2 [142], are topics that are beyond the scope of this review but nevertheless provide important evidence showing that photorespiration is not a wasteful process. There are many promising directions for further studies on photorespiration; for example, examining Mn^{2+} interactions with Rubisco, further exploring the reassimilation of photorespired CO_2, and exploring how the biochemical processes related to photorespiration contribute to its role in adaptation to various conditions will probably reveal that plant carbon fixation and respiration is more energy efficient than what has been previously assumed.

Author Contributions: Conceptualization, X.S. and A.B.; X.S.; writing—original draft preparation, X.S.; writing—review and editing, A.B.; visualization, X.S. and A.B.; supervision, A.B.; funding acquisition, A.B. All authors have read and agreed to the published version of the manuscript.

Funding: This work was funded in part by USDA-IWYP-16-06702, NSF grants IOS-16-55810 and CHE-19- 04310, and the John B. Orr Endowment.

Conflicts of Interest: The authors declare no conflict of interest.

References

1. Zelitch, I. Photorespiration: Studies with Whole Tissues. *Photosynthesis II* **1979**, *28*, 353–354.
2. Canvin, D.T. Photorespiration: Comparison Between C3 and C4 Plants. *Photosynthesis II* **1979**, *29*, 368–396.
3. Husic, D.W.; Husic, H.D.; Tolbert, N.E.; Black, C.C. The oxidative photosynthetic carbon cycle or C_2 cycle. *Crit. Rev. Plant Sci.* **1987**, *5*, 45–99. [CrossRef]
4. Sharkey, T.D. Estimating the rate of photorespiration in leaves. *Physiol. Plant* **1988**, *73*, 147–152. [CrossRef]
5. Ogren, W.L. Photorespiration: Pathways, Regulation, and Modification. *Annu. Rev. Plant Physiol.* **1984**, *35*, 415–442. [CrossRef]
6. Somerville, C.R.; Ogren, W.L. A phosphoglycolate phosphatase-deficient mutant of Arabidopsis. *Nature* **1979**, *280*, 833–836. [CrossRef]
7. Busch, F.A. Photorespiration in the context of Rubisco biochemistry, CO_2 diffusion and metabolism. *Plant J.* **2020**, *101*, 919–939. [CrossRef]
8. Bloom, A.J.; Lancaster, K.M. Manganese binding to Rubisco could drive a photorespiratory pathway that increases the energy efficiency of photosynthesis. *Nat. Plants* **2018**, *4*, 414–422. [CrossRef]
9. Bloom, A.J.; Smart, D.R.; Nguyen, D.T.; Searles, P.S. Nitrogen assimilation and growth of wheat under elevated carbon dioxide. *Proc. Natl. Acad. Sci. USA* **2002**, *99*, 1730–1735. [CrossRef]
10. McFadden, G.I. Origin and Evolution of Plastids and Photosynthesis in Eukaryotes. *Cold Spring Harb. Perspect. Biol.* **2014**, *6*, a016105. [CrossRef] [PubMed]
11. Raven, J.A. Rubisco: Still the most abundant protein of Earth? *New Phytol.* **2013**, *198*, 1–3. [CrossRef]
12. Badger, M.R.; Bek, E.J. Multiple Rubisco forms in proteobacteria: Their functional significance in relation to CO_2 acquisition by the CBB cycle. *J. Exp. Bot.* **2008**, *59*, 1525–1541. [CrossRef]
13. Kono, T.; Mehrotra, S.; Endo, C.; Kizu, N.; Matusda, M.; Kimura, H.; Mizohata, E.; Inoue, T.; Hasunuma, T.; Yokota, A.; et al. A RuBisCO-mediated carbon metabolic pathway in methanogenic archaea. *Nat. Commun.* **2017**, *8*, 14007. [CrossRef]
14. Tabita, F.R.; Satagopan, S.; Hanson, T.E.; Kreel, N.E.; Scott, S.S. Distinct form I, II, III, and IV Rubisco proteins from the three kingdoms of life provide clues about Rubisco evolution and structure/function relationships. *J. Exp. Bot.* **2007**, *59*, 1515–1524. [CrossRef]
15. Ogawa, S.; Suzuki, Y.; Yoshizawa, R.; Kanno, K.; Makino, A. Effect of individual suppression of RBCS multigene family on Rubisco contents in rice leaves. *Plant Cell Environ.* **2011**, *35*, 546–553. [CrossRef] [PubMed]
16. Bracher, A.; Whitney, S.M.; Hartl, F.U.; Hayer-Hartl, M. Biogenesis and Metabolic Maintenance of Rubisco. *Annu. Rev. Plant Biol.* **2007**, *68*, 29–60. [CrossRef] [PubMed]
17. Aigner, H.; Wilson, R.H.; Bracher, A.; Calisse, L.; Bhat, J.Y.; Hartl, F.U.; Hayer-Hartl, M. Plant RuBisCo assembly in E. coli with five chloroplast chaperones including BSD2. *Science* **2017**, *358*, 1272–1278. [CrossRef]
18. Foyer, C.H.; Bloom, A.J.; Queval, G.; Noctor, G. Photorespiratory metabolism: Genes, mutants, energetics, and redox signaling. *Annu. Rev. Plant Biol.* **2009**, *60*, 455–484. [CrossRef]
19. Betti, M.; Bauwe, H.; Busch, F.A.; Fernie, A.R.; Keech, O.; Levey, M.; Ort, D.R.; Parry MA, J.; Sage, R.; Timm, S.; et al. Manipulating photorespiration to increase plant productivity: Recent advances and perspectives for crop improvement. *J. Exp. Bot.* **2016**, *67*, 2977–2988. [CrossRef]
20. Walker, B.J.; VanLoocke, A.; Bernacchi, C.J.; Ort, D.R. The Costs of Photorespiration to Food Production Now and in the Future. *Annu. Rev. Plant Biol.* **2016**, *67*, 107–129. [CrossRef] [PubMed]
21. Pierce, J.; Andrews, T.J.; Lorimer, G.H. Reaction intermediate partitioning by ribulose-bisphosphate carboxylases with differing substrate specificities. *J. Biol. Chem.* **1986**, *261*, 10248–10256. [CrossRef]

22. Miziorko, H.M.; Sealy, R.C. Characterization of the ribulosebisphosphate carboxylase-carbon dioxide-divalent cation-carboxypentitol bisphosphate complex. *Biochemistry* **1980**, *19*, 1167–1171. [CrossRef] [PubMed]
23. Stec, B. Structural mechanism of RuBisCO activation by carbamylation of the active site lysine. *Proc. Natl. Acad. Sci. USA* **2012**, *109*, 18785–18790. [CrossRef] [PubMed]
24. Andrews, T.J.; Lorimer, G.H. *The Biochemistry of Plants: A Comprehensive Treatise*; Photosynthesis; Academic Press: San Diego, CA, USA, 1987; Volume 10.
25. Wildner, G.F.; Henkel, J. The effect of divalent metal ions on the activity of Mg(++) depleted ribulose-1,5-bisphosphate oxygenase. *Planta* **1979**, *146*, 223–228. [CrossRef] [PubMed]
26. Matsumura, H.; Mizohata, E.; Ishida, H.; Kogami, A.; Ueno, T.; Makino, A.; Inoue, T.; Yokota, A.; Mae, T.; Kai, Y. Crystal structure of rice Rubisco and implications for activation induced by positive effectors NADPH and 6-phosphogluconate. *Curr. Opin. Plant Biol.* **2012**, *422*, 75–86. [CrossRef] [PubMed]
27. Chollet, R.; Anderson, L.L. Regulation of ribulose 1,5-bisphosphate carboxylase-oxygenase activities by temperature pretreatment and chloroplast metabolites. *Arch. Biochem. Biophys.* **1976**, *176*, 344–351. [CrossRef]
28. McCurry, S.D.; Pierce, J.; Tolbert, N.E.; Orme-Johnson, W.H. On the mechanism of effector-mediated activation of ribulose bisphosphate carboxylase/oxygenase. *J. Biol. Chem.* **1981**, *256*, 6623–6628. [CrossRef]
29. Chu, D.K.; Bassham, J.A. Activation of ribulose 1,5-diphosphate carboxylase by nicotinamide adenine dinucleotide phosphate and other chloroplast metabolites. *Plant Physiol.* **1974**, *54*, 556–559. [CrossRef]
30. Hanson, T.E.; Satagopan, S.; Witte, B.H.; Kreel, N.E. Phylogenetic and evolutionary relationships of RubisCO and the RubisCO-like proteins and the functional lessons provided by diverse molecular forms. *Philos. Trans R. Soc. Lond. B Biol. Sci.* **2008**, *363*, 2629–2640.
31. Tcherkez GG, B.; Farquhar, G.D.; Andrews, T.J. Despite slow catalysis and confused substrate specificity, all ribulose bisphosphate carboxylases may be nearly perfectly optimized. *Proc. Natl. Acad. Sci. USA* **2006**, *103*, 7246–7251. [CrossRef]
32. Bloom, A.J.; Kameritsch, P. Relative association of Rubisco with manganese and magnesium as a regulatory mechanism in plants. *Physiol. Plant* **2017**, *161*, 545–559. [CrossRef]
33. Pierce, J.; Reddy, G.S. The sites for catalysis and activation of ribulosebisphosphate carboxylase share a common domain. *Arch. Biochem. Biophys.* **1986**, *245*, 483–493. [CrossRef]
34. Jordan, D.B.; Ogren, W.L. Species variation in kinetic properties of ribulose 1,5-bisphosphate carboxylase/oxygenase. *Arch. Biochem. Biophys.* **1983**, *227*, 425–433. [CrossRef]
35. Martin, F.; Winspear, M.J.; MacFarlane, J.D.; Oaks, A. Effect of Methionine Sulfoximine on the Accumulation of Ammonia in C3 and C4 Leaves. *Plant Physiol.* **1983**, *71*, 177–181. [CrossRef] [PubMed]
36. Christeller, J.T. The effects of bivalent cations on ribulose bisphosphate carboxylase/oxygenase. *Biochem. J.* **1981**, *193*, 839–844. [CrossRef] [PubMed]
37. Christeller, J.T.; Laing, W.A. Effects of manganese ions and magnesium ions on the activity of soya-bean ribulose bisphosphate carboxylase/oxygenase. *Biochem. J.* **1979**, *183*, 747–750. [CrossRef] [PubMed]
38. Jordan, D.B.; Ogren, W.L. A Sensitive Assay Procedure for Simultaneous Determination of Ribulose-1,5-bisphosphate Carboxylase and Oxygenase Activities. *Plant Physiol.* **1981**, *67*, 237–245. [CrossRef]
39. Lilley, R.M.; Wang, X.; Krausz, E.; Andrews, T.J. Complete spectra of the far-red chemiluminescence of the oxygenase reaction of Mn^{2+}-activated ribulose-bisphosphate carboxylase/oxygenase establish excited Mn^{2+} as the source. *J. Biol. Chem.* **2003**, *278*, 16488–16493. [CrossRef] [PubMed]
40. Mogel, S.N.; McFadden, B.A. Chemiluminescence of the Mn^{2+}-activated ribulose-1,5-bisphosphate oxygenase reaction: Evidence for singlet oxygen production. *Biochemistry* **1990**, *29*, 8333–8337. [CrossRef]
41. Bock, C.R.; Connor, J.A.; Gutierrez, A.R. Estimation of excited-state redox potentials by electron-transfer quenching. Application of electron-transfer theory to excited-state redox processes. *J. Am. Chem. Soc.* **1979**, *101*, 4815–4824. [CrossRef]
42. Creutz, C.; Sutin, N. Reaction of tris(bipyridine)ruthenium(III) with hydroxide and its application in a solar energy storage system. *Proc. Natl. Acad. Sci. USA* **1975**, *72*, 2858–2862. [CrossRef]
43. Sattler, W.; Ener, M.E.; Blakemore, J.D. Generation of powerful tungsten reductants by visible light excitation. *J. Am. Chem. Soc.* **2013**, *135*, 10614–10617. [CrossRef] [PubMed]
44. Müller, G.L.; Drincovich, M.F.; Andreo, C.S.; Lara, M.V. Nicotiana tabacum NADP-malic enzyme: Cloning, characterization and analysis of biological role. *Plant Cell Physiol.* **2008**, *49*, 469–480. [CrossRef] [PubMed]
45. Wheeler MC, G.; Arias, C.L.; Tronconi, M.A.; Maurino, V.G.; Andreo, C.S.; Drincovitch, M.F. Arabidopsis thaliana NADP-malic enzyme isoforms: High degree of identity but clearly distinct properties. *Plant Mol. Biol.* **2008**, *67*, 231–242. [CrossRef]
46. Husic, H.D.; Tolbert, N.E. Anion and divalent cation activation of phosphoglycolate phosphatase from leaves. *Arch. Biochem. Biophys.* **1984**, *229*, 64–72. [CrossRef]
47. Decker, J.P. A Rapid, Postillumination Deceleration of Respiration in Green Leaves. *Plant Physiol.* **1955**, *30*, 82–84. [CrossRef]
48. Peterson, R.B. Estimation of Photorespiration Based on the Initial Rate of Postillumination CO_2 Release: I. A Nonsteady State Model for Measurement of CO_2 Exchange Transients. *Plant Physiol.* **1983**, *73*, 978–982. [CrossRef]
49. Laisk, A.; Kiirats, O.; Oja, V. Assimilatory Power (Postillumination CO_2 Uptake) in Leaves. *Plant Physiol.* **1984**, *76*, 723–729. [CrossRef]
50. Sharkey, T.D.; Seemann, J.R.; Pearcy, R.W. Contribution of Metabolites of Photosynthesis to Postillumination CO_2 Assimilation in Response to Lightflects. *Plant Physiol.* **1986**, *82*, 1063–1068. [CrossRef]

51. Azcón-Bieto, J.; Osmond, C.B. Relationship between Photosynthesis and Respiration: The Effect of Carbohydrate Status on the Rate of CO_2 Production by Respiration in Darkened and Illuminated Wheat Leaves. *Plant Physiol.* **1983**, *71*, 574–581. [CrossRef] [PubMed]
52. Sharkey, T.D. O_2-Insensitive Photosynthesis in C3 Plants. *Plant Physiol.* **1985**, *78*, 71–75. [CrossRef]
53. Caemmerer, S.V.; Edmondson, D.L. Relationship Between Steady-State Gas Exchange, in vivo Ribulose Bisphosphate Carboxylase Activity and Some Carbon Reduction Cycle Intermediates in Raphanus sativus. *Funct. Plant Biol.* **1986**, *13*, 669–688. [CrossRef]
54. Badger, M.R.; Sharkey, T.D.; von Caemmerer, S. The relationship between steady-state gas exchange of bean leaves and the levels of carbon-reduction-cycle intermediates. *Planta* **1984**, *160*, 305–313. [CrossRef] [PubMed]
55. Ludwig, L.J.; Canvin, D.T. An open gas-exchange system for the simultaneous measurement of the CO_2 and $^{14}CO_2$ fluxes from leaves. *Can. J. Bot.* **1971**, *49*, 1299–1313. [CrossRef]
56. Gerbaud, A.; Andre, M. An Evaluation of the Recycling in Measurements of Photorespiration. *Plant Physiol.* **1987**, *83*, 933–937. [CrossRef] [PubMed]
57. O'Leary, M.H. Carbon isotope fractionation in plants. *Phytochemistry* **1981**, *20*, 553–567. [CrossRef]
58. Farquhar, G.D.; von Caemmerer, S. Modelling of Photosynthetic Response to Environmental Conditions. *Physiol. Plant Ecol. II* **1982**, *12*, 549–587.
59. Busch, F.A. Current methods for estimating the rate of photorespiration in leaves. *Plant Biol.* **2012**, *15*, 648–655. [CrossRef]
60. Busch, F.A.; Sage, T.L.; Cousins, A.B.; Sage, R.F. C3 plants enhance rates of photosynthesis by reassimilating photorespired and respired CO_2. *Plant Cell Environ.* **2012**, *36*, 200–212. [CrossRef]
61. Parnik, T.; Keerberg, O. Decarboxylation of primary and end products of photosynthesis at different oxygen concentrations. *J. Exp. Bot.* **1995**, *46*, 1439–1477. [CrossRef]
62. Pärnik, T.; Keerberg, O. Advanced radiogasometric method for the determination of the rates of photorespiratory and respiratory decarboxylations of primary and stored photosynthates under steady-state photosynthesis. *Physiol. Plant* **2007**, *129*, 34–44. [CrossRef]
63. Ivanova, H.; Keerberg, O. Photorespiratory and respiratory decarboxylations in leaves of C3 plants under different CO_2 concentrations and irradiances. *Plant Cell Environ.* **2007**, *30*, 1535–1544.
64. Tcherkez, G.; Mahé, A.; Guérard, F.; Boex-Fontvieille, E.R.A.; Gout, E.; Lamothe, M.; Barbour, M.M.; Bligny, R. Short-term effects of CO_2 and O_2 on citrate metabolism in illuminated leaves. *Plant Cell Environ.* **2012**, *35*, 2208–2220. [CrossRef] [PubMed]
65. Bauwe, H.; Hagemann, M.; Fernie, A.R. Photorespiration: Players, partners and origin. *Trends Plant Sci.* **2010**, *15*, 330–336. [CrossRef] [PubMed]
66. Lacuesta, M.; Dever, L.V.; Munoz-Rueda, A.; Lea, P.J. A study of photorespiratory ammonia production in the C4 plant Amaranthus edulis, using mutants with altered photosynthetic capacities. *Physiol. Plant* **1997**, *99*, 447–455. [CrossRef]
67. Wendler, C.; Barniske, M.; Wild, A. Effect of phosphinothricin (glufosinate) on photosynthesis and photorespiration of C3 and C4 plants. *Planta* **1990**, *24*, 55–61. [CrossRef]
68. Husted, S.; Hebbern, C.A.; Mattsson, M. A critical experimental evaluation of methods for determination of NH_4^+ in plant tissue, xylem sap and apoplastic fluid. *Physiol. Plant* **2000**, *109*, 167–179. [CrossRef]
69. Ruuska, S.A.; Badger, M.R.; Andrews, T.J.; Von Caemmerer, S. Photosynthetic electron sinks in transgenic tobacco with reduced amounts of Rubisco: Little evidence for significant Mehler reaction. *J. Exp. Bot.* **2000**, *51*, 357–368. [CrossRef]
70. Canvin, D.T.; Berry, J.A.; Badger, M.R.; Fock, H.; Osmond, C.B. Oxygen Exchange in Leaves in the Light. *Plant Physiol.* **1980**, *66*, 302–307. [CrossRef]
71. De Veau, E.J.; Burris, J.E. Photorespiratory rates in wheat and maize as determined by o-labeling. *Chem. Rev.* **1989**, *90*, 500–511. [CrossRef]
72. Berry, J.A.; Osmond, C.B.; Lorimer, G.H. Fixation of O_2 during Photorespiration: Kinetic and Steady-State Studies of the Photorespiratory Carbon Oxidation Cycle with Intact Leaves and Isolated Chloroplasts of C3 Plants. *Plant Physiol.* **1978**, *62*, 954–967. [CrossRef]
73. Cegelski, L.; Schaefer, J. Glycine Metabolism in Intact Leaves by in Vivo ^{13}C and ^{15}N Labeling. *J. Biol. Chem.* **2005**, *280*, 39238–39245. [CrossRef]
74. Arrivault, S.; Guenther, M.; Fry, S.C.; Fuenfgeld, M.M.; Veyel, D.; Mettler-Altmann, T.; Stitt, M.; Lunn, J.E. Synthesis and Use of Stable-Isotope-Labeled Internal Standards for Quantification of Phosphorylated Metabolites by LC–MS/MS. *Biochemistry* **2015**, *87*, 6896–6904. [CrossRef] [PubMed]
75. Fernie, A.R.; Bauwe, H. *Photorespiration: Methods and Protocols*; Humana Press: Totowa, NJ, USA, 2017.
76. Arrivault, S.; Guenther, M.; Ivakov, A.; Feil, R.; Vosloh, D.; van Dongen, J.T.; Sulpice, R.; Stitt, M. Use of reverse-phase liquid chromatography, linked to tandem mass spectrometry, to profile the Calvin cycle and other metabolic intermediates in Arabidopsis rosettes at different carbon dioxide concentrations. *Plant J.* **2009**, *59*, 826–839. [CrossRef] [PubMed]
77. Nunes, A. Is there a metabolic requirement for photorespiratory enzyme activities in heterotrophic tissues? *Mol. Plant* **2014**, *7*, 248–251. [CrossRef]
78. Mintz-Oron, S.; Meir, S.; Malitsky, S.; Ruppin, E.; Aharoni, A.; Shlomi, T. Reconstruction of Arabidopsis metabolic network models accounting for subcellular compartmentalization and tissue-specificity. *Proc. Natl. Acad. Sci. USA* **2011**, *109*, 339–344. [CrossRef] [PubMed]

79. Lernmark, U.; Henricson, D.; Wigge, B.; Gardestrom, P. Glycine oxidation in mitochondria isolated from light grown and etiolated plant tissue. *Physiol. Plant* **1991**, *82*, 339–344. [CrossRef]
80. Jacoby, R.P.; Millar, A.H.; Taylor, N.L. Application of selected reaction monitoring mass spectrometry to field-grown crop plants to allow dissection of the molecular mechanisms of abiotic stress tolerance. *Front. Plant Sci.* **2013**, *4*. [CrossRef] [PubMed]
81. Igamberdiev, A.U.; Bykova, N.V. Involvement of cyanide-resistant and rotenone-insensitive pathways of mitochondrial electron transport during oxidation of glycine in higher plants. *FEBS Lett.* **1997**, *412*, 265–269. [CrossRef]
82. Trufelli, H.; Palma, P.; Famiglini, G. An overview of matrix effects in liquid chromatography–mass spectrometry. *Mass Spectrom. Rev.* **2011**, *30*, 491–509. [CrossRef]
83. Tohge, T.; Mettler, T.; Arrivault, S.; Carroll, A.J. From models to crop species: Caveats and solutions for translational metabolomics. *Front. Plant Sci.* **2011**, *2*, 61. [CrossRef] [PubMed]
84. King, R.; Bonfiglio, R.; Fernandez, C. Mechanistic investigation of ionization suppression in electrospray ionization. *J. Am. Soc. Mass Spectrom.* **2000**, *11*, 942–950. [CrossRef]
85. Bonfiglio, R.; King, R.C.; Olah, T.V. The effects of sample preparation methods on the variability of the electrospray ionization response for model drug compounds. *Rapid Commun. Mass Spectrom.* **1999**, *13*, 1175–1185. [CrossRef]
86. Römisch-Margl, W.; Schramek, N.; Radykewicz, T.; Ettenhuber, C.; Eylert, E.; Huber, C.; Römisch-Margl, L.; Schwarz, C.; Dobner, M.; Demmel, N.; et al. $^{13}CO_2$ as a universal metabolic tracer in isotopologue perturbation experiments. *Phytochemistry* **2007**, *68*, 2273–2289. [CrossRef]
87. Eisenreich, W.; Bacher, A. Advances of high-resolution NMR techniques in the structural and metabolic analysis of plant biochemistry. *Phytochemistry* **2007**, *68*, 2799–2815. [CrossRef] [PubMed]
88. Heise, R.; Arrivault, S.; Szecowka, M.; Tohge, T.; Nunes-Nesi, A.; Stitt, M.; Nikoloski, Z.; Fernie, A.R. Flux profiling of photosynthetic carbon metabolism in intact plants. *Nat. Protoc.* **2014**, *9*, 1803–1824. [CrossRef] [PubMed]
89. Ma, F.; Jazmin, L.J.; Young, J.D.; Allen, D.K. Isotopically nonstationary ^{13}C flux analysis of changes in Arabidopsis thaliana leaf metabolism due to high light acclimation. *Proc. Natl. Acad. Sci. USA* **2014**, *111*, 16967–16972. [CrossRef] [PubMed]
90. Szecowka, M.; Heise, R.; Tohge, T.; Nunes-Nesi, A.; Vosloh, D.; Huege, J.; Feil, R.; Lunn, J.; Nikoloski, Z.; Stitt, M.; et al. Metabolic Fluxes in an Illuminated Arabidopsis Rosette. *Plant Cell* **2013**, *25*, 694–714. [CrossRef]
91. Adebiyi, A.O.; Jazmin, L.J.; Young, J.D. ^{13}C flux analysis of cyanobacterial metabolism. *Photosyn. Res.* **2014**, *126*, 19–32. [CrossRef]
92. Cheah, Y.E.; Young, J.D. Isotopically nonstationary metabolic flux analysis (INST-MFA): Putting theory into practice. *Curr. Opin. Biotechnol.* **2018**, *54*, 80–87. [CrossRef]
93. Clark, L.C.; Wolf, R.; Granger, D.; Taylor, Z. Continuous recording of blood oxygen tensions by polarography. *J. Appl. Physiol.* **1953**, *6*, 189–193. [CrossRef]
94. Severinghaus, J.W.; Astrup, P.B. History of blood gas analysis. IV. Leland Clark's oxygen electrode. *J. Clin. Monit.* **1986**, *2*, 125–139. [CrossRef]
95. Bittig, H.C.; Körtzinger, A.; Neill, C.; van Ooijen, E.; Plant, J.N.; Hahn, J.; Johnson, K.S.; Yang, B.; Emerson, S.R. Oxygen Optode Sensors: Principle, Characterization, Calibration, and Application in the Ocean. *Front. Mar. Sci.* **2018**, *4*, 429. [CrossRef]
96. Fischer, M.; Falke, D.; Pawlik, T.; Sawers, R.G. Oxygen-dependent control of respiratory nitrate reduction in mycelium of Streptomyces coelicolor A3(2). *J. Bacteriol.* **2014**, *196*, 4152–4162. [CrossRef]
97. Flitsch, D.; Ladner, T.; Lukacs, M.; Büchs, J. Easy to use and reliable technique for online dissolved oxygen tension measurement in shake flasks using infrared fluorescent oxygen-sensitive nanoparticles. *Microb. Cell Fact.* **2016**, *15*, 1–11. [CrossRef] [PubMed]
98. Helm, I.; Karina, G.; Jalukse, L.; Pagano, T.; Leito, I. Comparative validation of amperometric and optical analyzers of dissolved oxygen: A case study. *Environ. Monit. Assess* **2018**, *190*, 1–18. [CrossRef] [PubMed]
99. Bentzon-Tilia, M.; Severin, I.; Hansen, L.H.; Riemann, L. Genomics and Ecophysiology of Heterotrophic Nitrogen-Fixing Bacteria Isolated from Estuarine Surface Water. *mBio* **2015**, *6*. [CrossRef] [PubMed]
100. Ortner, A.; Huber, D.; Haske, O. Laccase mediated oxidation of industrial lignins: Is oxygen limiting? *Process Biochem.* **2015**, *50*, 1277–1283. [CrossRef]
101. Bloom, A.J. Photorespiration and nitrate assimilation: A major intersection between plant carbon and nitrogen. *Photosyn. Res.* **2014**, *123*, 117–128. [CrossRef]
102. Bloom, A.J.; Burger, M.; Asensio, J.S.; Cousins, A.B. Carbon dioxide enrichment inhibits nitrate assimilation in wheat and Arabidopsis. *Science* **2010**, *328*, 899–903. [CrossRef]
103. Aranjuelo, I.; Cabrerizo, P.M.; Arrese, C. Pea plant responsiveness under elevated [CO_2] is conditioned by the N source (N_2 fixation versus NO_3^- fertilization). *Environ. Exp. Bot.* **2013**, *95*, 34–40. [CrossRef]
104. Rachmilevitch, S.; Cousins, A.B.; Bloom, A.J. Nitrate assimilation in plant shoots depends on photorespiration. *Proc. Natl. Acad. Sci. USA* **2004**, *101*, 11506–11510. [CrossRef]
105. Lekshmy, S.; Jain, V.; Khetarpal, S.; Pandey, R. Inhibition of nitrate uptake and assimilation in wheat seedlings grown under elevated CO_2. *Indian J. Plant Physiol.* **2013**, *18*, 23–29. [CrossRef]
106. Pleijel, H.; Uddling, J. Yield vs. quality trade-offs for wheat in response to carbon dioxide and ozone. *Glob. Chang. Biol.* **2011**, *18*, 596–605. [CrossRef]
107. Bloom, A.J.; Asensio JS, R.; Randall, L.; Rachmilevitch, S.; Cousins, A.B.; Carlisle, E.A. CO_2 enrichment inhibits shoot nitrate assimilation in C3 but not C4 plants and slows growth under nitrate in C3 plants. *Ecology* **2012**, *93*, 355–367. [CrossRef]

108. Carlisle, E.; Myers, S.S.; Raboy, V.; Bloom, A.J. The effects of inorganic nitrogen form and CO_2 concentration on wheat yield and nutrient accumulation and distribution. *Front. Plant Sci.* **2012**, *3*, 195. [CrossRef] [PubMed]
109. Bloom, A.J.; Burger, M.; Kimball, B.A.; Pinter, P.J., Jr. Nitrate assimilation is inhibited by elevated CO_2 in field-grown wheat. *Nat. Clim. Chang.* **2014**, *4*, 477–480. [CrossRef]
110. Carlisle, E.; Yarnes, C.; Toney, M.D.; Bloom, A.J. Nitrate reductase ^{15}N discrimination in *Arabidopsis thaliana*, *Zea mays*, *Aspergillus niger*, *Pichea angusta*, and *Escherichia coli*. *Front. Plant Sci.* **2014**, *5*, 317. [CrossRef]
111. Warburg, O. Assimilatory quotient and photochemical yield. *Am. J. Bot.* **1948**, *35*, 194–204. [CrossRef] [PubMed]
112. Bloom, A.J.; Caldwell, R.M.; Finazzo, J.; Warner, R.L. Oxygen and carbon dioxide fluxes from barley shoots depend on nitrate assimilation. *Plant Physiol.* **1989**, *91*, 352–356. [CrossRef]
113. Cen, Y.P.; Turpin, D.H.; Layzell, D.B. Whole-plant gas exchange and reductive biosynthesis in white lupin. *Plant Physiol.* **2001**, *126*, 1555–1565. [CrossRef]
114. Matt, P.; Geiger, M.; Walch-Liu, P.; Engels, C. Elevated carbon dioxide increases nitrate uptake and nitrate reductase activity when tobacco is growing on nitrate, but increases ammonium uptake and inhibits nitrate reductase activity when tobacco is growing on ammonium nitrate. *Plant Cell Environ.* **2011**, *24*, 1119–1137. [CrossRef]
115. Passama, L.; Gojon, A.; Robin, P.; Salsac, L. In situ nitrate reductase activity as an indicator of nitrate availability. *Plant Soil* **1987**, *102*, 145–148. [CrossRef]
116. Kaiser, W.M.; Kandlbinder, A.; Stoimenova, M.; Glaab, J. Discrepancy between nitrate reduction rates in intact leaves and nitrate reductase activity in leaf extracts: What limits nitrate reduction in situ? *Planta* **2000**, *210*, 801–807. [CrossRef] [PubMed]
117. Wilkinson, J.Q.; Crawford, N.M. Identification and characterization of a chlorate-resistant mutant of Arabidopsis thaliana with mutations in both nitrate reductase structural genes NIA1 and NIA2. *Mol. Gen. Genet.* **1993**, *239*, 289–297. [CrossRef] [PubMed]
118. Warner, R.L.; Kleinhofs, A. Nitrate utilization by nitrate reductase-deficient barley mutants. *Plant Physiol.* **1981**, *67*, 740–743. [CrossRef] [PubMed]
119. Eichelberger, K.D.; Lambert, R.J.; Below, F.E. Divergent phenotypic recurrent selection for nitrate reductase activity in maize. II. Efficient use of fertilizer nitrogen. *Crop Sci.* **1989**, *29*, 1398–1402. [CrossRef]
120. Andrews, M.; Condron, L.M.; Kemp, P.D.; Topping, J.F. Elevated CO_2 effects on nitrogen assimilation and growth of C_3 vascular plants are similar regardless of N-form assimilated. *J. Exp. Bot.* **2019**, 683–690. [CrossRef] [PubMed]
121. Andrews, M.; Condron, L.M.; Kemp, P.D. Will rising atmospheric CO_2 concentration inhibit nitrate assimilation in shoots but enhance it in roots of C3 plants? *Physiol. Plant* **2020**, *170*, 40–45. [CrossRef]
122. Obata, T.; Florian, A.; Timm, S.; Bauwe, H.; Fernie, A.R. On the metabolic interactions of (photo)respiration. *J. Exp. Bot.* **2016**, *67*, 3003–3014. [CrossRef]
123. Scheibe, R. Malate valves to balance cellular energy supply. *Physiol. Plant* **2004**, *120*, 21–26. [CrossRef] [PubMed]
124. Voss, I.; Sunil, B.; Scheibe, R.; Raghavendra, A.S. Emerging concept for the role of photorespiration as an important part of abiotic stress response. *Plant Biol.* **2013**, *15*, 713–722. [CrossRef]
125. Taniguchi, M.; Miyake, H. Redox-shuttling between chloroplast and cytosol: Integration of intra-chloroplast and extra-chloroplast metabolism. *Curr. Opin. Plant Biol.* **2012**, *15*, 252–260. [CrossRef] [PubMed]
126. Backhausen, J.E.; Emmerlich, A.; Holtgrefe, S.; Horton, P.; Nast, G.; Rogers, J.J.; Müller-Röber, B.; Scheibe, R. Transgenic potato plants with altered expression levels of chloroplast NADP-malate dehydrogenase: Interactions between photosynthetic electron transport and malate metabolism in leaves and in isolated intact chloroplasts. *Planta* **1998**, *207*, 105–114. [CrossRef]
127. Bloom, A.J. The increasing importance of distinguishing among plant nitrogen sources. *Curr. Opin. Plant. Biol.* **2015**, *25*, 10–16. [CrossRef] [PubMed]
128. Dutilleul, C.; Lelarge, C.; Prioul, J.-L.; De Paepe, R.; Foyer, C.H.; Noctor, G. Mitochondria-driven changes in leaf NAD status exert a crucial influence on the control of nitrate assimilation and the integration of carbon and nitrogen metabolism. *Plant Physiol.* **2005**, *139*, 64–78. [CrossRef]
129. Schneidereit, J.; Häusler, R.E.; Fiene, G.; Kaiser, W.M.; Weber AP, M. Antisense repression reveals a crucial role of the plastidic 2-oxoglutarate/malate translocator DiT1 at the interface between carbon and nitrogen metabolism. *Plant J.* **2005**, *45*, 206–224. [CrossRef]
130. Cossins, E.A. The fascinating world of folate and one-carbon metabolism. *Can. J. Bot.* **2000**, *78*, 691–708.
131. Hanson, A.D.; Roje, S. One-carbon metabolism in higher plants. *Annu. Rev. Plant Physiol. Plant Mol. Biol.* **2001**, *52*, 119–137. [CrossRef]
132. Crider, K.S.; Yang, T.P.; Berry, R.J.; Bailey, L.B. Folate and DNA methylation: A review of molecular mechanisms and the evidence for folate's role. *Adv. Nutr.* **2012**, *3*, 21–38. [CrossRef]
133. Gorelova, V.; Ambach, L.; Rébeillé, F.; Stove, C.; Van Der Straeten, D. Folates in Plants: Research Advances and Progress in Crop Biofortification. *Front. Chem.* **2017**, *5*, 21. [CrossRef] [PubMed]
134. Abadie, C.; Tcherkez, G. Plant sulphur metabolism is stimulated by photorespiration. *Commun. Biol.* **2019**, *2*, 1–7. [CrossRef]
135. Tcherkez, G.; Tea, I. $^{32}S/^{34}S$ isotope fractionation in plant sulphur metabolism. *New Phytol.* **2013**, *200*, 44–53. [CrossRef]
136. Amrani, A.; Kamyshny, A.; Lev, O.; Aizenshtat, Z. Sulfur Stable Isotope Distribution of Polysulfide Anions in an $(NH_4)_2Sn$ Aqueous Solution. *Inorg. Chem.* **2006**, *45*, 1427–1429. [CrossRef]
137. Rausch, T.; Wachter, A. Sulfur metabolism: A versatile platform for launching defence operations. *Trends Plant Sci.* **2005**, *10*, 503–509. [CrossRef] [PubMed]

138. Cantoni, G.L. The nature of the active methyl donor formed enzymatically from L-methionine and adenosine triphosphate[1,2]. *J. Am. Chem. Soc.* **1952**, *74*, 2942–2943. [CrossRef]
139. Timm, S.; Bauwe, H. The variety of photorespiratory phenotypes—Employing the current status for future research directions on photorespiration. *Plant Biol.* **2013**, *15*, 737–747. [CrossRef]
140. Eisenhut, M.; Ruth, W.; Haimovich, M.; Bauwe, H.; Kaplan, A.; Hagemann, M. The photorespiratory glycolate metabolism is essential for cyanobacteria and might have been conveyed endosymbiontically to plants. *Proc. Natl. Acad. Sci. USA* **2008**, *105*, 17199–17204. [CrossRef]
141. Eisenhut, M.; Bräutigam, A.; Timm, S.; Florian, A.; Tohge, T. Photorespiration is crucial for dynamic response of photosynthetic metabolism and stomatal movement to altered CO_2 availability. *Mol. Plant* **2017**, *10*, 47–61. [CrossRef]
142. Ziotti, A.; Silva, B.P.; Neto, M. Photorespiration is crucial for salinity acclimation in castor bean. *Environ. Exp. Bot.* **2019**, *167*, 103845. [CrossRef]